ChemElectroChem

Research Article
doi.org/10.1002/celc.202300659

Chemistry Europe
European Chemical Societies Publishing

www.chemelectrochem.org

Strain-Dependent Activity-Stability Relations in RuO_2 and IrO_2 Oxygen Evolution Catalysts

Payal Chaudhary,[a] Alexandra Zagalskaya,[a, b] Herbert Over,[c] and Vitaly Alexandrov*[a]

Strain engineering is an effective strategy in modulating activity of electrocatalysts, but the effect of strain on electrochemical stability of catalysts remains poorly understood. In this work, we combine *ab initio* thermodynamics and molecular dynamics simulations to examine the role of compressive and tensile strain in the interplay between activity and stability of metal oxides considering RuO_2 and IrO_2 as exemplary catalysts. We reveal that although compressive strain leads to improved activity via the adsorbate-evolving mechanism of the oxygen evolution reaction, even small strains should substantially destabilize these catalysts promoting dissolution of transition metals. In contrast, our results show that the metal oxides requiring tensile strain to promote their catalytic activity may also benefit from enhanced stability. Importantly, we also find that the detrimental effect of strain on electrochemical stability of atomically flat surfaces could be even greater than that of surface defects.

Introduction

Strain engineering is an established strategy to modify the electronic structure of electrocatalysts allowing one to tune the binding energy of rate-limiting reaction intermediates and thereby enhance catalytic performance.[1–11] Electrocatalytic activity as a function of adsorption strength of key reaction intermediates is typically expressed in the form of a volcano plot similar to the one shown in Scheme 1A. For example, $LaNiO_3$ requires compressive strain to improve its OER activity by driving it to the top of the volcano plot,[12] whereas $LaCoO_3$ needs tensile strain to enhance OER activity.[6] Overall, this approach has been demonstrated for a wide range of (electro)catalytic materials and reactions. Importantly, it was also shown that the applied stress can break linear scaling relations between adsorption energies of reaction intermediates and thus allow larger changes in reaction rates.[13]

There exist various sources of strain that can be favorably exploited in electrocatalysis. One common approach to create compressive or tensile strain in the host material is to introduce transition metals with smaller or larger atomic radii, respectively. This can be achieved by synthesizing core-shell nanostructures.[14–17] Strain can also emerge as a result of adsorption of reaction intermediates, the presence of structural defects, and nanostructuring of catalysts.[10] In addition, potential cycling, either to deliberately steer electrocatalytic activity[18] or due to the potentiodynamic operation of an electrochemical device,[19–21] may lead to accumulation of lattice strain. In this process, the kinetics of metal oxidation (or metal-oxide reduction), surface restructuring and the rate of potential cycling will lead to an interplay between strain accumulation and release affecting overall electrochemical stability. In particular, the electronic structure of a catalyst will change in response to the dynamically changing potential, but surface restructuring may be relatively slow in adopting the most favorable atomic configuration under specific potential.

In the past years, there have been also substantial efforts in understanding strain effects in electrocatalysis. Crucially, it was demonstrated that lattice strain affects not only binding strength of adsorbates, but also a variety of other key properties such as charge transport and magnetism,[22] defect formation energy,[23] and surface oxygen exchange kinetics.[24] One critical property of electrocatalysts is their long-term electrochemical stability. Therefore, the last decade has seen a significant upsurge of interest in understanding activity-stability relationships across electrocatalytic systems.[25–33] However, our current knowledge on the extent to which lattice strain can compromise electrochemical stability of catalysts remains limited.

In this study, we employ density functional theory (DFT) calculations to investigate the role of lattice strain in affecting catalytic activity and electrochemical stability considering rutile-type RuO_2 and IrO_2 as representative oxygen evolution reaction (OER) electrocatalysts. This work is driven by two major hypotheses that are schematically shown in Scheme 1. First, we argue that there should be an intrinsic relationship between activity of a metal-oxide catalyst towards a certain electrochemical reaction and the propensity of a catalyst to undergo transition-metal dissolution to aqueous solution under applied strain (see Scheme 1A). Specifically, compressive strain leading to shorter metal-oxygen bonds should promote the formation

[a] P. Chaudhary, Dr. A. Zagalskaya, Prof. Dr. V. Alexandrov
Department of Chemical and Biomolecular Engineering, University of Nebraska-Lincoln, Lincoln, Nebraska 68588, United States
E-mail: valexandrov2@unl.edu

[b] Dr. A. Zagalskaya
Quantum Simulations Group, Materials Science Division, Lawrence Livermore National Laboratory, Livermore, CA, 94550, United States

[c] Prof. Dr. H. Over
Institute of Physical Chemistry, Justus Liebig University, 35392 Giessen, Germany

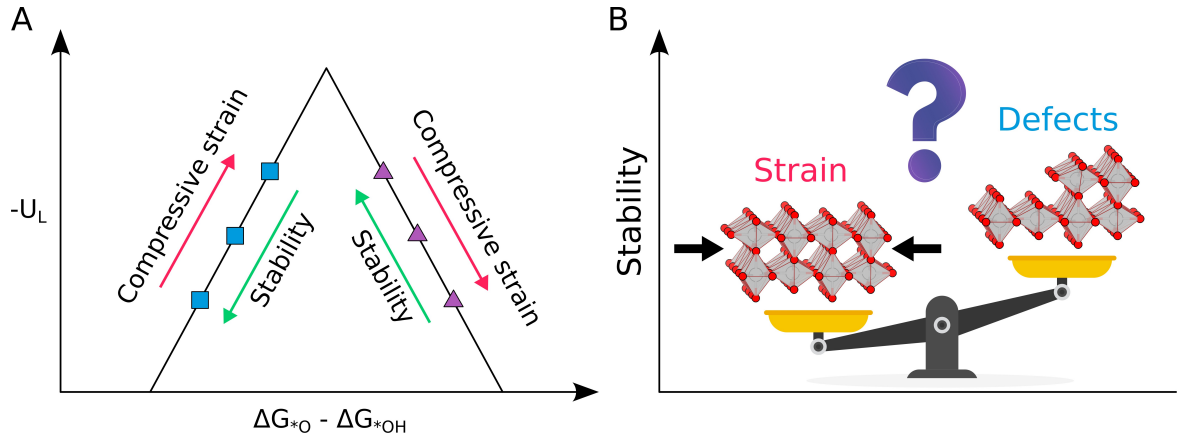

Scheme 1. Scheme summarizing two research hypotheses for the intrinsic relationship between activity and stability of metal-oxide catalysts: A) The activity volcano plot shows that if a catalyst requires compressive strain to climb to the top of the volcano (the left leg), then it should lead to destabilization of transition-metal species in the oxide lattice promoting their dissolution in higher oxidation states. In contrast, catalysts requiring tensile strain to enhance their activity (the right leg) may benefit from improved stability. B) The plot shows the possibility of small strain imposed to promote catalytic activity to be more detrimental to electrochemical stability than the presence of surface defects.

of transition-metal species in higher oxidation states at the surface (i.e., Ru^{5+} and Ir^{5+} in the case of RuO_2 and IrO_2) that are more prone to dissolution. Therefore, it could be expected that electrochemical stability of metal-oxide catalysts that require compressive strain to improve their activity would be compromised. In contrast, if tensile strain is necessary to enhance catalytic activity, then metal-oxide stability might be improved. Here, we assume that applied strains are sufficiently small to cause surface restructuring. Our second hypothesis (see Scheme 1B) is that the effect of the imposed strain on materials stability might be comparable or even greater than that of surface defects that are commonly considered as the sites at which materials corrosion is initiated. This hypothesis is based on the fact that even small strains of several percent of a lattice constant may result in substantial weakening of surface metal-oxygen bonds.[9,34]

To address these hypotheses, we perform systematic DFT simulations of the effects of compressive and tensile strain on OER activity and electrochemical stability of the rutile-type RuO_2 and IrO_2(110) surfaces. To evaluate OER activity by calculating thermodynamic overpotentials, we employ the computational hydrogen electrode (CHE) approach.[35] Electrochemical stability is analyzed by computing the formation energies for transition-metal vacancies and estimating kinetic barriers of transition-metal dissolution by means of *ab initio* molecular dynamics (AIMD) based thermodynamic integration (blue moon ensemble).

Results and Discussion

First, we analyze the OER activity as a function applied epitaxial strain considering both the conventional adsorbate-evolving (AEM) and lattice-oxygen (LOM) mechanisms.[26,36,37] The AEM and LOM reaction pathways on the rutile MO_2(110) surface are illustrated in Figure 1 where the active sites are highlighted

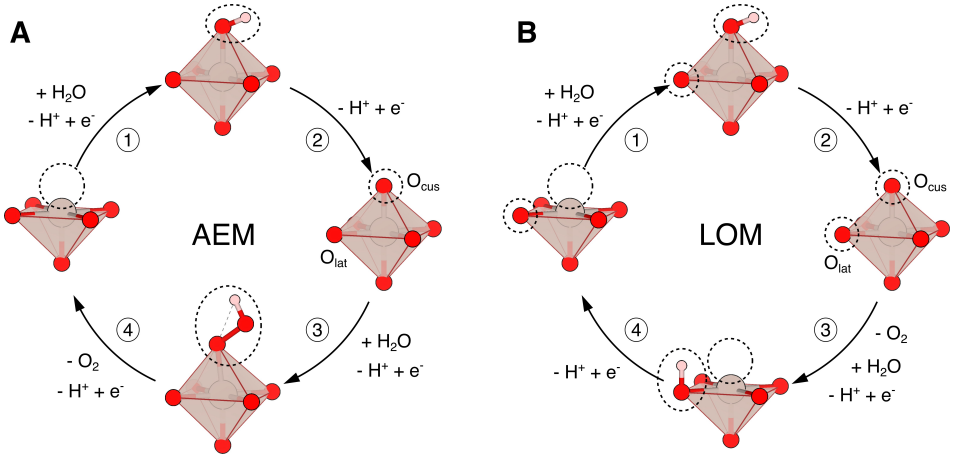

Figure 1. A) AEM and B) LOM reaction mechanisms of the OER analyzed in this study.

with dotted circles. We note that O_{cus} are the reaction sites for the conventional AEM mechanism, whereas the lattice O sites (O_{lat}) participate in the LOM of the OER. We observe that when tensile strain is applied, i.e. when the M–O_{lat} bond lengths increase, the M–O_{cus} bonds become shorter for both IrO_2 and RuO_2. Conversely, when compressive strain is applied and M–O_{lat} bonds become shorter, M–O_{cus} bonds get slightly elongated. This has important implications for the OER activity via the AEM and LOM pathways as discussed below.

Figure 2 shows DFT calculated overpotentials for the AEM and LOM mechanisms as a function of imposed strain relative to the unstrained catalysts. We note that in the case of IrO_2 under compressive strain larger than 2% the H-site reaction intermediate formed during the LOM turns out to be unstable as the proton spontaneously moves from O_{lat} to O_{cus} during optimization. This precludes the calculation of the LOM overpotentials, and so we are only plotting the LOM results up to 2% strains. As seen from the figure, under compressive strain AEM activity (expressed in terms of thermodynamic overpotential η_{AEM}) increases, while LOM activity decreases for both catalysts. On the other hand, under tensile strain AEM activity decreases and LOM activity improves. This theoretical finding appears to be consistent with the experimental observation of pH dependence for unstrained RuO_2 suggesting some contribution of LOM and the lack of thereof in strained RuO_2 suggesting that the major contribution comes from the AEM mechanism.[38]

We further find that there is a clear correlation between the shifts of the O-2*p* band center as a function of applied strain for the O_{cus} and O_{lat} sites and OER activity (see Figure 3). Specifically, we observe that with increasing strain, the O_{cus}-2*p* band centers become lower in energy indicating that the O_{cus} atoms should be less OER active. On the other hand, the O_{lat}-2*p* band centers are found to increase in energy thereby becoming closer the Fermi level suggesting higher OER activity.[39] This is consistent with the results presented in Figure 4 showing a nearly linear correlation between the change in OER activity as measured by thermodynamic overpotentials with the change in O-2*p* band centers. One can clearly see that as the O-2*p* band center increases, the overpotential (η) decreases suggesting greater OER activity. With an increase of tensile strain, AEM overpotentials increase and O_{cus}-2*p* band centers decrease. For LOM overpotentials and O_{lat}-2*p* band centers, the opposite is

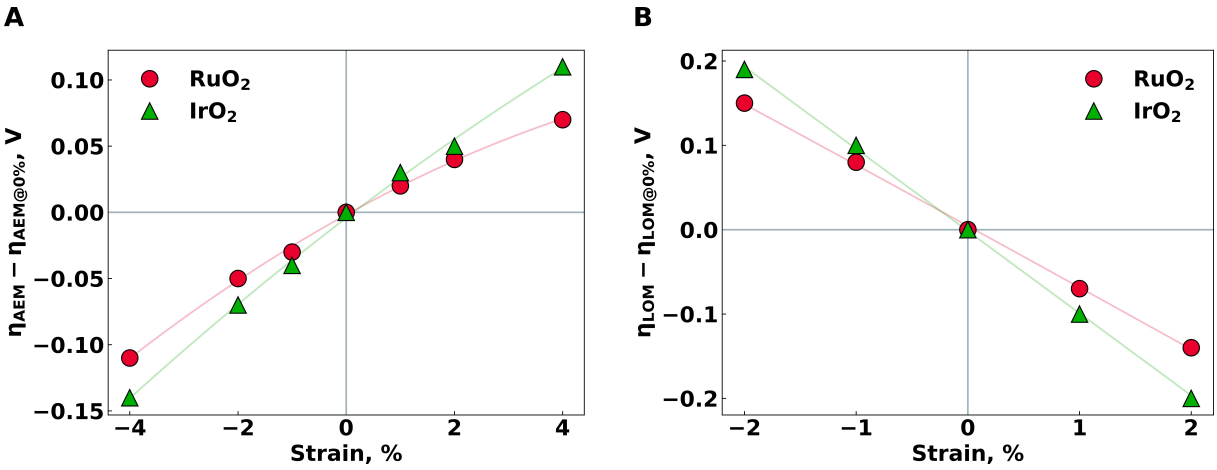

Figure 2. A) AEM (η_{AEM}) and B) LOM (η_{LOM}) overpotentials as a function of applied strain relative to the values for the unstrained systems ($\eta_{AEM@0\%}$ and $\eta_{LOM@0\%}$). The plots demonstrate the opposite activity trends for the AEM and LOM mechanisms of the OER under strain.

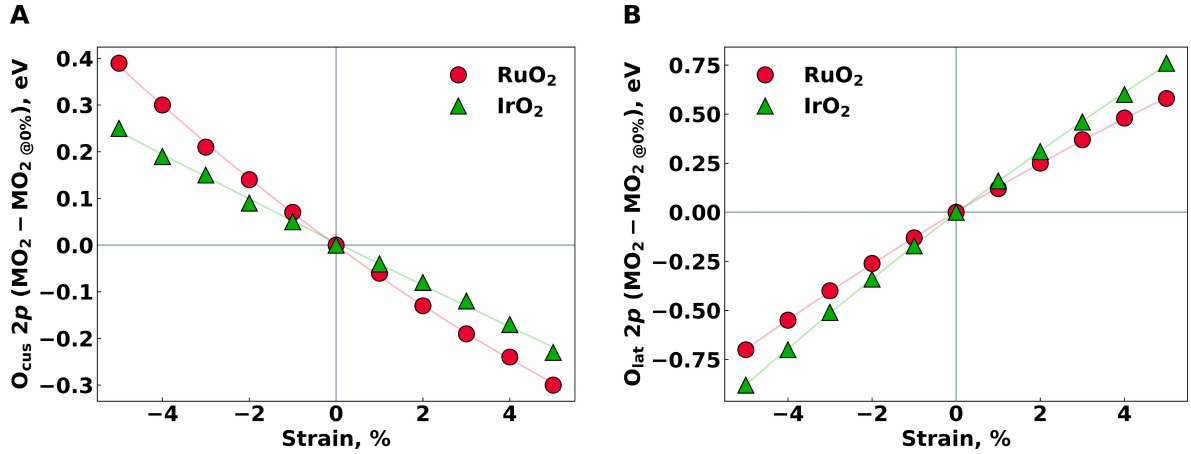

Figure 3. Change in O_{cus} and O_{lat} 2*p* band centers at the reaction sites vs strain relative to the values for the unstrained systems.

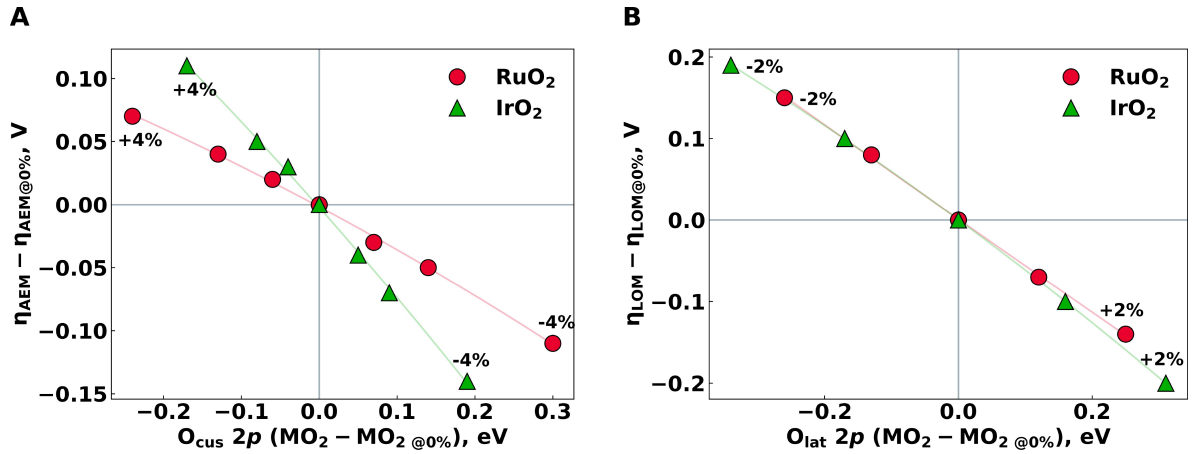

Figure 4. AEM (η_{AEM}) and LOM (η_{LOM}) overpotentials relative to the values for the unstrained systems ($\eta_{AEM@0\%}$ and $\eta_{LOM@0\%}$) vs. O_{cus}-2*p* and O_{lat}-2*p* band centers. The annotated labels indicate the strain values.

true. Upon increasing tensile strain, O_{lat} sites become more reactive towards OER and LOM overpotentials are found to reduce.

We next analyze the effect of applied strain on stability of RuO_2 and IrO_2 catalysts and how it relates to the OER activity. First of all, we calculate the Bader charges (*q*) on the surface transition-metal atoms for the unstrained and strained oxides. We find that *q*(Ru) changes from 1.97 (−4%) through 1.91 (0%) to 1.84 (+4%), while *q*(Ir) changes from 1.92 (−4%), through 1.90 (0%) to 1.79 (+4%) as a function of applied strain. This trend is consistent with Shannon ionic radii for species in different oxidation states. We then calculate transition-metal vacancy formation energies at the catalyst surface as a function of applied strain (see Figure 5). We observe that the formation of a metal vacancy becomes much more favorable under compressive strain relative to the unstrained case, while the opposite trend is observed for the tensile strain. This is consistent with inducing higher oxidation states on transition metals for the compressed structures and suggests a significant thermodynamic driving force for transition metals to dissolve. It is now instructive to compare these formation energies with those obtained for some defective but unstrained surfaces. Here, we chose both the regular (110) surface and a (120) step derived from the rutile MO_2(110) surface as a representative defective surface that can be formed during dissolution (see the atomic structures in Figure 6).[26,40] It can be seen from Table 1 that the formation energies of transition-metal vacancies in the compressively strained oxides are much lower than those for the defective unstrained surfaces.

To provide insights into dissolution behavior of compressively strained RuO_2 and IrO_2 beyond thermodynamics, we also evaluate transition-metal dissolution kinetics by employing AIMD thermodynamic integration calculations. Figure 7 shows the dissolution profiles emerged from these AIMD dissolution simulations. We note that the statistical errors associated with

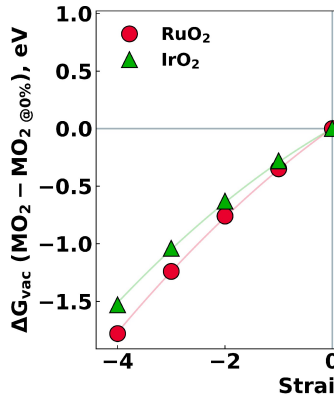

Figure 5. Formation energy for a single transition-metal vacancy on the flat (110) surface of RuO_2 and IrO_2 as a function of applied strain.

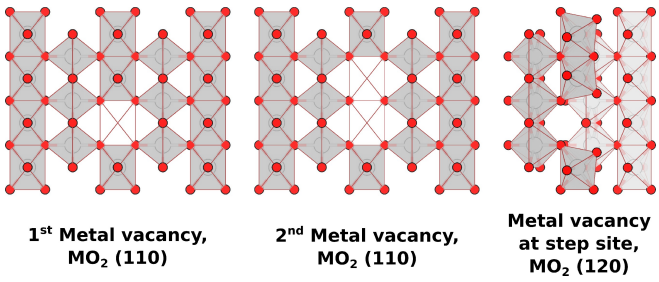

Figure 6. Atomic structures for the one and two transition-metal vacancies created on the MO_2(110) surface, as well as one vacancy on the (120) step.

Table 1. Metal vacancy (M_{vac}) formation energies for the unstrained and strained regular (110) surface, as well as for the (120) step (see the corresponding atomic structures in Figure 6) computed relative to the unstrained system with one M_{vac}.

	Unstrained			-4% strain	+4% strain
	1st M_{vac}	2nd M_{vac}	M_{vac} at (120) step	1st M_{vac}	1st M_{vac}
RuO_2	0.00 eV	−0.20 eV	1.29 eV	−1.78 eV	0.89 eV
IrO_2	0.00 eV	0.91 eV	2.32 eV	−1.53 eV	0.63 eV

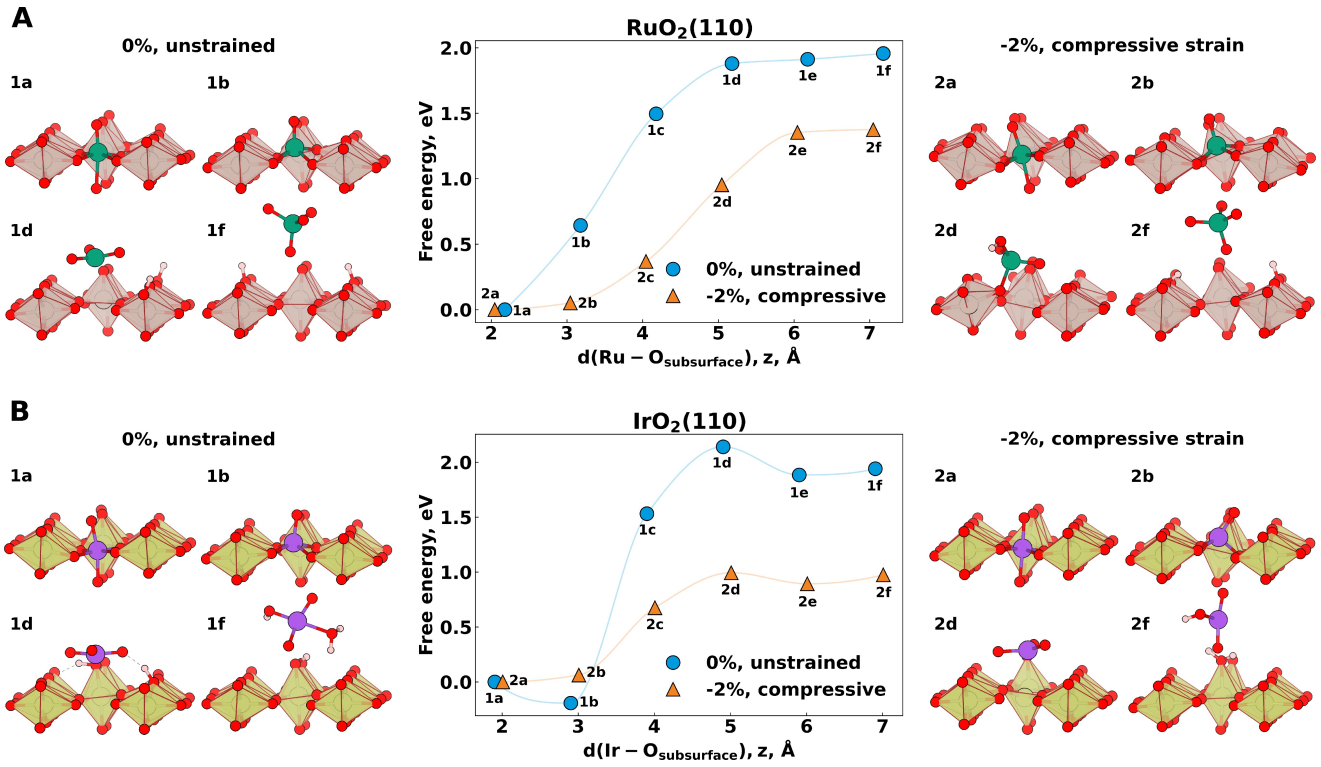

Figure 7. Free-energy profiles (in the center) derived from blue moon AIMD simulations for transition-metal dissolution from the unstrained and 2% compressively strained RuO_2 (A) and IrO_2 (B) (110) surfaces into aqueous solution. Key dissolution intermediates along each dissolution trajectory are also shown with solution water species removed for clarity.

such calculations were previously estimated using the block-averaging approach not to exceed 10%.[27,41] Here, the profiles for the 0% unstrained structure and the one with the moderate 2% compressive strain are compared. Key dissolution intermediates along the dissolution pathways are also depicted. It can be seen that, in agreement with previous AIMD simulations,[42–45] the final transition-metal dissolution products are RuO_4 and IrO_2OH. We observe that compressive strain has a huge effect on transition-metal dissolution kinetics being qualitatively consistent with our DFT thermodynamics data on the metal vacancy formation (Table 1). In particular, the free energy barriers are found to be almost twice smaller for the 2% compressively strained oxides relative to the unstrained systems. We note here that the absolute values of the dissolution barriers are likely to be overestimated due to the incorrect description of the formation energetics for the dissolution products at the DFT-GGA level.[40] Nevertheless, comparing the energy profiles between the unstrained and strained systems should provide reasonable trends. We also want to point out that Raman et al.[44] previously used *ab initio* steered molecular dynamics and umbrella sampling methods to compute dissolution profiles for partially protonated RuO_2 and IrO_2(110) surfaces rather than fully oxidized facets. As a result, they reported much higher barriers of 3.4 eV for the dissolution of the cus Ru site to $RuO_2(OH)_2$ and 4.6 eV for the dissolution of the cus Ir site to IrO_2OH.

It is a common practice now to benchmark electrochemical stability of OER catalysts using the stability number as a metric.[46] This stability number is defined as the ratio between the amounts of oxygen evolved via OER and dissolved transition metal. This definition enables a reasonable comparison of stability across various electrocatalysts. We note that it is not straightforward to quantitatively relate our DFT data with such stability numbers. Moreover, our results suggest that compressively strained RuO_2 and IrO_2 films should exhibit both higher OER activity and greater dissolution propensity. Therefore, it is not obvious how applied compressive strains will quantitatively affect stability numbers of RuO_2 and IrO_2. On the other hand, it might be hypothesized that if tensile strain is required to promote OER activity of a metal-oxide catalyst, then its stability number will be increased.

We also would like to comment that transition-metal dissolution triggered by the strain may lead to some strain relaxation at the surface via the formation of surface metal vacancies. This could potentially make the effect self-terminating. On the other hand, however, our thermodynamic estimates presented above suggest that strained systems may have higher thermodynamic propensity for dissolution that defective structures. Therefore, it might be hypothesized that strained systems may exhibit a more uniform rather than more localized dissolution of transition metals.

Conclusions

In conclusion, we have employed DFT simulations to study the role of lattice strain in electrocatalytic activity and stability of rutile-structured RuO_2 and IrO_2 serving as representative OER metal-oxide electrocatalysts. As our model systems, we have considered the effects of compressive and tensile strains on both the adsorbate evolving (AEM) and lattice-oxygen (LOM) mechanisms of the OER, as well as on transition-metal dissolution from the (110) surface into aqueous solution. Our simulations have provided several key insights into the interplay between activity and stability properties of metal-oxide catalysts. First, we determine that the imposed lattice strain leads to the opposite reactivity trends for the two OER pathways (AEM and LOM) for the considered systems. Second, we have demonstrated that even small compressive strains can significantly compromise stability of metal oxides promoting transition-metal dissolution from the flat non-defective surfaces into an aqueous solution. Thus, we have revealed that activity and stability characteristics can be simultaneously enhanced by the applied strain if tensile strain is required to promote catalytic activity. Also, our results suggest that the quantitative effect of lattice strain on electrochemical stability of atomically flat surfaces might be comparable to that of the defective surfaces such as those exposing step and kink sites. We believe that our results on the relationship between OER activity and transition-metal dissolution as a function of lattice strain are generalizable to metal-oxide systems and electrocatalytic reactions beyond OER-active RuO_2 and IrO_2.

Computational Details

Density functional theory (DFT) calculations were performed using the Vienna Ab initio Simulation Package (VASP).[47,48] The projector augmented wave (PAW) potentials (Ir, Ru_pv, O, H) were employed[49] and exchange-correlation functionals were described using the revised PBE (RPBE) scheme.[50] Non-local van der Waals interactions were described using the DFT–D3 method based on Grimme's formalism.[51] A plane-wave cutoff energy of 400 eV was used in all calculations. Smearing was introduced using the first-order Methfessel-Paxton method with a smearing width of 0.2 eV. The *k*-point mesh for each structure was generated using the VASPKIT code[52] with the Monkhorst-Pack *k*-mesh scheme and a *k*-mesh resolved value of $2\pi\times0.02$ Å. The truncation criteria for electronic steps was chosen to be 10^{-6} eV.

The rutile MO_2(110) (M=Ir, Ru) surfaces were modeled as periodic four-layer slabs with a 2×3 surface supercell (12.67×9.33 Å^2 for unstrained RuO_2 and 12.76×9.54 Å^2 for unstrained IrO_2) and a vacuum gap of about 10 Å. The lattice parameters for the unstrained bulk unit cell were taken from the Materials Project website. A uniform lattice strain was introduced along all three axes in the bulk unit cell, and subsequently slab models were generated for values ranging from −4% to 4% strain of the lattice constant. The atomic positions of OER intermediates and CUS oxygen atoms were optimized, and all other atoms were kept fixed.

Ab initio molecular dynamics (AIMD) simulations were performed to model transition-metal dissolution. Similar to the methodology applied in a series of previous studies,[26,42,53] we compared −2% (compressive) and 0% (unstrained) strained structures using AIMD thermodynamic integration method. The simulations were run at the Γ point within the Born-Oppenheimer dynamics framework as implemented in the VASP code. The vacuum was filled with 27 explicit water molecules to obtain water density of around 1 g/cm^3. The slab/water systems were equilibrated for at least 20 ps, and the atomic positions of the bottom two layers were kept fixed. The distance between the surface metal atom (Ru or Ir) and the subsurface O was used as a collective variable to push the metal atom away from the slab at a velocity of 0.5 Å/ps to determine the sequence of M–O bond-breaking events. Subsequently, the thermodynamic integration approach was employed within the blue moon ensemble method to obtain accurate free energy barriers ($\Delta G^{\#}$) between the intermediate states along each metal dissolution pathway. The atomic configuration in each window was equilibrated for 3 ps, followed by force averaging done over a 2 ps timeframe. A time step of 1.0 fs and the H mass of 3 amu were set. A truncation criteria of 10^{-4} eV was used for electronic steps in all AIMD simulations. The Nose-Hoover thermostat was chosen to keep the temperature around 300 K in our simulations.

Acknowledgements

VA acknowledges funding support from the National Science Foundation (NSF) through the NSF CAREER award (Grant No. CBET-1941204). HO acknowledges financial support from the Deutsche Forschungsgemeinschaft (DFG, German Researcjh foundation – 493681475). This research used resources of the National Energy Research Scientific Computing Center, a DOE Office of Science User Facility supported by the Office of Science of the U.S. Department of Energy under Contract No. DE-AC02-05CH11231, as well as the Holland Computing Center at the University of Nebraska-Lincoln.

Conflict of Interests

The authors declare no conflict of interest.

Data Availability Statement

The data that support the findings of this study are available from the corresponding author upon reasonable request.

Keywords: Lattice strain · Oxygen evolution reaction · Stability · Electrocatalysis · Metal oxide catalysts

[1] V. Jalan, E. J. Taylor, *J. Electrochem. Soc.* **1983**, *130*, 2299.
[2] M. Mavrikakis, B. Hammer, J. K. Nørskov, *Phys. Rev. Lett.* **1998**, *81*, 2819.
[3] P. Strasser, S. Koh, T. Anniyev, J. Greeley, K. More, C. Yu, Z. Liu, S. Kaya, D. Nordlund, H. Ogasawara, M. F. Toney, A. Nilsson, *Nat. Chem.* **2010**, *2*, 454.
[4] I. E. L. Stephens, A. S. Bondarenko, U. Grønbjerg, J. Rossmeisl, I. Chorkendorff, *Energy Environ. Sci.* **2012**, *5*, 6744.
[5] J. Wu, P. Li, Y.-T. F. Pan, S. Warren, X. Yin, H. Yang, *Chem. Soc. Rev.* **2012**, *41*, 8066.
[6] K. A. Stoerzinger, W. S. Choi, H. Jeen, H. N. Lee, Y. Shao-Horn, *J. Phys. Chem. Lett.* **2015**, *6*, 487.
[7] M. Luo, S. Guo, *Nat. Rev. Mater.* **2017**, *2*, 17059.

[8] R. P. Jansonius, L. M. Reid, C. N. Virca, C. P. Berlinguette, *ACS Energy Lett.* **2019**, *4*, 980.
[9] J. Hwang, Z. Feng, N. Charles, X. R. Wang, D. Lee, K. A. Stoerzinger, S. Muy, R. R. Rao, D. Lee, R. Jacobs, D. Morgan, Y. Shao-Horn, *Mater. Today* **2019**, *31*, 100.
[10] X. Yang, Y. Wang, X. Tong, N. Yang, *Adv. Energy Mater.* **2022**, *12*, 2102261.
[11] Z. Hou, C. Cui, Y. Li, Y. Gao, D. Zhu, Y. Gu, G. Pan, Y. Zhu, T. Zhang, *Adv. Mater.* **2023**, *n/a*, 2209876.
[12] J. R. Petrie, V. R. Cooper, J. W. Freeland, T. L. Meyer, Z. Zhang, D. A. Lutterman, H. N. Lee, *J. Am. Chem. Soc.* **2016**, *138*, 2488.
[13] A. Khorshidi, J. Violet, J. Hashemi, A. A. Peterson, *Nat. Catal.* **2018**, *1*, 263.
[14] R. Ghosh Chaudhuri, S. Paria, *Chem. Rev.* **2012**, *112*, 2373.
[15] M. B. Gawande, A. Goswami, T. Asefa, H. Guo, A. V. Biradar, D.-L. Peng, R. Zboril, R. S. Varma, *Chem. Soc. Rev.* **2015**, *44*, 7540.
[16] J. T. Gamler, A. Leonardi, X. Sang, K. M. Koczkur, R. R. Unocic, M. Engel, S. E. Skrabalak, *Nanoscale Adv.* **2020**, *2*, 1105.
[17] M. Liu, M. Xie, Y. Jiang, Z. Liu, Y. Lu, S. Zhang, Z. Zhang, X. Wang, K. Liu, Q. Zhang, T. Cheng, C. Gao, *J. Mater. Chem. A* **2021**, *9*, 15373.
[18] J. Timoshenko, A. Bergmann, C. Rettenmaier, A. Herzog, R. M. Arán-Ais, H. S. Jeon, F. T. Haase, U. Hejral, P. Grosse, S. Kühl, E. M. Davis, J. Tian, O. Magnussen, B. Roldan Cuenya, *Nat. Catal.* **2022**, *5*, 259.
[19] R. Chattot, I. Martens, M. Mirolo, M. Ronovsky, F. Russello, H. Isern, G. Braesch, E. Hornberger, P. Strasser, E. Sibert, M. Chatenet, V. Honkimäki, J. Drnec, *J. Am. Chem. Soc.* **2021**, *143*, 17068.
[20] F. D. Speck, A. Zagalskaya, V. Alexandrov, S. Cherevko, *Angew. Chem. Int. Ed.* **2021**, *60*, 13343.
[21] A. Zagalskaya, P. Chaudhary, V. Alexandrov, *J. Phys. Chem. C* **2023**, *127*, 14587.
[22] J. M. Rondinelli, N. A. Spaldin, *Phys. Rev. B* **2009**, *79*, 054409.
[23] M. G. Sensoy, D. Vinichenko, W. Chen, C. M. Friend, E. Kaxiras, *Phys. Rev. B* **2017**, *95*, 014106.
[24] M. Kubicek, Z. Cai, W. Ma, B. Yildiz, H. Hutter, J. Fleig, *ACS Nano* **2013**, *7*, 3276.
[25] O. Kasian, J.-P. Grote, S. Geiger, S. Cherevko, K. J. J. Mayrhofer, *Angew. Chem. Int. Ed.* **2018**, *57*, 2488.
[26] A. Zagalskaya, V. Alexandrov, *ACS Catal.* **2020**, *10*, 3650.
[27] A. Zagalskaya, I. Evazzade, V. Alexandrov, *ACS Energy Lett.* **2021**, *6*, 1124.
[28] S. Czioska, A. Boubnov, D. Escalera-López, J. Geppert, A. Zagalskaya, P. Röse, E. Saraçi, V. Alexandrov, U. Krewer, S. Cherevko, J.-D. Grunwaldt, *ACS Catal.* **2021**, *11*, 10043.
[29] H. Over, *ACS Catal.* **2021**, *11*, 8848.
[30] A. R. Zeradjanin, J. Masa, I. Spanos, R. Schlögl, *Front. Energy Res.* **2021**, *8*.
[31] F. Zeng, C. Mebrahtu, L. Liao, A. K. Beine, R. Palkovits, *J. Energy Chem.* **2022**, *69*, 301.
[32] F. Hess, *Curr. Opin. Electrochem.* **2023**, *41*, 101349.
[33] A. Zagalskaya, M. R. Nouri, V. Alexandrov, *Curr. Opin. Electrochem.* **2023**, *41*, 101352.
[34] D. Ma, Z. Lu, Y. Tang, T. Li, Z. Tang, Z. Yang, *Phys. Lett. A* **2014**, *378*, 2570.
[35] J. K. Norskov, J. Rossmeisl, A. Logadottir, L. Lindqvist, J. R. Kitchin, T. Bligaard, H. Jonsson, *J. Phys. Chem. B* **2004**, *108*, 17886.
[36] A. Grimaud, O. Diaz-Morales, B. Han, W. T. Hong, Y.-L. Lee, L. Giordano, K. A. Stoerzinger, M. T. M. Koper, Y. Shao-Horn, *Nat. Chem.* **2017**, *9*, 457.
[37] N. Zhang, Y. Xiong, *J. Phys. Chem. C* **2023**, *127*, 2147.
[38] P. Adiga, W. Nunn, C. Wong, A. K. Manjeshwar, S. Nair, B. Jalan, K. A. Stoerzinger, *Mater. Today Energy* **2022**, *28*, 101087.
[39] A. Grimaud, K. J. May, C. E. Carlton, Y.-L. Lee, M. Risch, W. T. Hong, J. Zhou, Y. Shao-Horn, *Nat. Commun.* **2013**, *4*, 2439.
[40] C. F. Dickens, J. K. Nørskov, *J. Phys. Chem. C* **2017**, *121*, 18516.
[41] K. Klyukin, K. M. Rosso, V. Alexandrov, *J. Phys. Chem.* C **2018**, *122*, 16086.
[42] K. Klyukin, A. Zagalskaya, V. Alexandrov, *J. Phys. Chem. C* **2019**, *123*, 22151.
[43] A. Zagalskaya, V. Alexandrov, *J. Phys. Chem. Lett.* **2020**, *11*, 2695.
[44] A. S. Raman, A. Vojvodic, *J. Phys. Chem. C* **2022**, *126*, 922.
[45] F. Hess, H. Over, *ACS Catal.* **2023**, *13*, 3433.
[46] S. Geiger, O. Kasian, M. Ledendecker, E. Pizzutilo, A. M. Mingers, W. T. Fu, O. Diaz-Morales, Z. Li, T. Oellers, L. Fruchter, et al., *Nature Catalysis* **2018**, *1*, 508.
[47] G. Kresse, J. Furthmüller, *Phys. Rev. B* **1996**, *54*, 11169.
[48] G. Kresse, J. Furthmüller, *Comput. Mater. Sci.* **1996**, *6*, 15.
[49] G. Kresse, D. Joubert, *Phys. Rev. B* **1999**, *59*, 1758.
[50] J. P. Perdew, K. Burke, M. Ernzerhof, *Phys. Rev. Lett.* **1996**, *77*, 3865.
[51] S. Grimme, J. Antony, S. Ehrlich, H. Krieg, *J. Chem. Phys.* **2010**, *132*, 154104.
[52] V. Wang, N. Xu, J.-C. Liu, G. Tang, W.-T. Geng, *Comput. Phys. Commun.* **2021**, *267*, 108033.
[53] T. Bucko, *J. Phys. Condens. Matter* **2008**, *20*, 064211.

Manuscript received: November 10, 2023
Revised manuscript received: November 22, 2023
Version of record online: ■■, ■■

RESEARCH ARTICLE

Effect of strain on oxygen evolution activity and stability of RuO_2 and IrO_2 is investigated. Compressive strain has different effects depending on oxygen evolution pathways. Activity and stability can be simultaneously enhanced if tensile strain is required to promote catalytic activity. The quantitative effect of lattice strain on electrochemical stability of atomically flat surfaces might be comparable to that of defective surfaces.

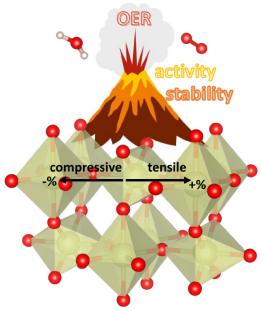

*P. Chaudhary, Dr. A. Zagalskaya, Prof. Dr. H. Over, Prof. Dr. V. Alexandrov**

1 – 8

Strain-Dependent Activity-Stability Relations in RuO_2 and IrO_2 Oxygen Evolution Catalysts